Chinese Chemical Letters 32 (2021) 2151–2154

Contents lists available at ScienceDirect

Chinese Chemical Letters

journal homepage: www.elsevier.com/locate/cclet

Communication

Amorphous carbon-linked TiO_2/carbon nanotube film composite with enhanced photocatalytic performance: The effect of interface contact and hydrophilicity

Zekun Xin[a], Xiaodong Zhao[a], Huiming Ji[a], Tianyi Ma[d], Hui Li[c,**], Shuhui Zhong[b,**], Zhurui Shen[a,c,*]

[a] School of Materials Science and Engineering, Key Laboratory of Advanced Ceramics and Machining Technology, Ministry of Education, Tianjin University, Tianjin 300350, China
[b] School of Mathematics, Tianjin University, Tianjin 300350, China
[c] School of Materials Science and Engineering, Nankai University, Tianjin 300350, China
[d] Centre for Translational Atomaterials, Faculty of Science, Engineering & Technology, Swinburne University of Technology, Hawthorn, Victoria 3122, Australia

ARTICLE INFO

Article history:
Received 21 September 2020
Received in revised form 23 October 2020
Accepted 13 November 2020
Available online 1 December 2020

Keywords:
Carbon nanotube film
TiO_2
Photocatalysis
Hydrophilia
Rhodamine B

ABSTRACT

Carbon nanotube film (CNTF) can be used for photocatalysis and water treatment due to its porous structure, good stability and excellent electrical properties. In this work, TiO_2/amorphous carbon/carbon nanotube film (TCC) composite with uniform structure was prepared by a simple atomization spraying method. Rhodamine B (RhB) was used to test the photocatalytic activity of TCC. TCC composite exhibits good photocatalytic activity under ultraviolet light. In particular, the degradation efficiency of rhodamine B (RhB) by TCC sprayed with 9 layers of TiO_2 (9TCC) increased by 1.45 times than of TiO_2 under ultraviolet light. The enhanced photocatalytic activity of TCC is attributed to the CNTF, which can broaden the light response range of TCC and improve the migration efficiency of electrons. The existence of amorphous carbon will promote these advances. Moreover, the better hydrophilic properties would enhance the catalytic performance happened on the solid-liquid interface. Finally, the photocatalytic mechanism and degradation intermediates of the TCC composite were proposed.

Water pollution caused by industrialization has been recognized as a severe challenge in the 21st century [1]. Organic dye pollution has caused great concern due to its widespread application in industry. The discharge of high-color sewage can reduce the penetration of light, thereby reducing the ability of algae to produce food and oxygen [2]. At present, using photocatalysts was proposed as an environmentally friendly potential strategy [3,4]. TiO_2, which is widely used in various fields, is nontoxicity, acid and alkali corrosion resistance and low cost [5]. However, the TiO_2 powder is easy to agglomerate and requires a long precipitation time and efficient solid-liquid separation technology [6]. In addition, the band gap of single-phase TiO_2 is around 3.2 eV, not sensitive to visible light which limits its development [7]. Consequently, designing new TiO_2-based photocatalysts to inhibit agglomeration, facilitate separation and improve photocatalytic activity is very attractive and challenging for sewage purification.

At present, loading TiO_2 on glass, silica and film materials is one of the most effective methods to inhibit agglomeration and facilitate separation [8], such as glass fiber, zeolite [9,10]. Compared with other substrates, thin film materials possess low density and can float on water, making it close to the air and water interface, enhancing the oxidation of the photocatalyst, which is a prerequisite for an efficient photocatalytic process [11]. Among these widely explored film substrates, CNTF displays excellent response to entire range from ultraviolet to infrared light [12,13], and its network channel can form an electrons transmission channel, appearing excellent electronic properties [14–16], which can be used to couple with TiO_2 to enhance light absorption, promote the separation of photogenerated electrons and holes and further improve photocatalytic activity.

In this work, the TCC composite was synthesized by a simple atomization spray method, using CNTF as the substrate and resin as

* Corresponding author at: School of Materials Science and Engineering, Key Laboratory of Advanced Ceramics and Machining Technology, Ministry of Education, Tianjin University, Tianjin 300350, China.
** Corresponding authors.
E-mail addresses: lihui@nankai.edu.cn (H. Li), zhshuhui@tju.edu.cn (S. Zhong), shenzhurui@nankai.edu.cn (Z. Shen).

https://doi.org/10.1016/j.cclet.2020.11.054
1001-8417/

the linking agent for TiO_2 spraying. TCC composite was annealed to carbonize the resin in the middle to amorphous carbon, coupling the titanium dioxide and improving the conductivity of electrons in the catalyst [17,18]. The TCC composite sprayed with nine layers of TiO_2 can degrade 91.29% of RhB within 120 min. The total organic carbon (TOC) content in the RhB solution before and after the reaction was detected. TCC composite can completely mineralize most of the RhB with a mineralization rate of 61.7%.

The crystal structure of TiO_2, CNTF and 9TCC were studied by XRD. As shown in Fig. S2a (Supporting information), the characteristic peaks of TiO_2 at $2\theta = 25.5^\circ$, 38.1°, 48.2°, 54.3° and 55.0° is corresponding to (101), (004), (200), (211) and (204) crystal planes of anatase TiO_2 respectively, which are consistent with JCPDS No. 21-1272 [19,20]. The diffraction peak of CNTF at $2\theta = 26.3^\circ$ is indexed to the (002) crystal plane of graphite material [21]. After coupled with TiO_2, the characteristic peak of TiO_2 in 9TCC can be observed. Since the peak of the carbon in 9TCC is not obvious, we carry out further tests on the CNTF and 9TCC through Raman analysis. In Fig. S2b (Supporting information), the peak of TiO_2 at 144.96 cm^{-1} (E_g), 639.37 cm^{-1} (E_g), 517.56 cm^{-1} (A_{1g}, B_{1g}) and 396.29 cm^{-1} (B_{1g}) can be clearly seen by the Raman spectrum of 9TCC, among which the characteristic peak of anatase TiO_2 can be obviously observed at 144.96 cm^{-1} [22,23]. In addition, the Raman spectroscopy is widely used to characterize the interaction of carbon materials with other substances. Peak D at 1358 cm^{-1} is the characteristic peak of defects around carbon atoms, and peak G at 1586 cm^{-1} is the stretching vibration of sp^2 hybridization of C atoms. The smaller the I_D/I_G, the higher degree of graphitization of carbon [24]. It can be observed from the Fig. S2b that the I_D/I_G of TCC is greater than that of CNTF, mainly due to the amorphous carbon formed after the resin carbonization.

The composition and valence of each element of 9TCC was monitored by the X-ray photoelectron spectroscopy (XPS) high-resolution spectrum analysis. It can be seen from the Fig. S2d (Supporting information) that there are four states of C. The binding energy from low to high is sp^2 and sp^3 hybridized C—C bond at 284.8 eV, C—O bond at 285. 8 eV, C—O—C bond at 286.7 eV, and C=O bond at 288.3 eV. The formation of these bonds are mainly due to resin cross linking [25]. In Fig. S2e (Supporting information), the peaks of 529.5 eV and 532.2 eV correspond to O in TiO_2 and O in Ti_2O_3, respectively. The peak of 531.1 eV can be attributed to the O—H bond of TiO_2 [26]. In addition, the spectrum of Ti 2p exhibits Ti $2p_{1/2}$ and Ti $2p_{3/2}$ energy levels. The difference of the two energy levels is 5.8 eV, which is consistent with the literature [27]. The C—O bonds are also observed in the FT-IR spectrum (Fig. S3 in Supporting information).

The microstructure of 9TCC was investigated by scanning electron microscopy (SEM) and transmission electron microscopy (TEM) analysis. Fig. 1a can observe the network structure of CNTF, and Figs. 1b-d are the SEM images of 3, 9 and 11 layers of TiO_2 sprayed. It can be concluded that the TiO_2 dispersion effect is better, and each particle is about 10−50 nm. While TiO_2 is uniformly loaded on the CNTF framework, it also has certain pores and sufficient reactive sites. With the growth of TiO_2, the TiO_2 particles that did not adhere to the resin began to agglomerate due to the high surface tension, as shown in Fig. 1d. We can observe from Fig. S4 (Supporting information) that TiO_2 is supported on CNTF. The lattice fringes of TiO_2 are clearly observed in Fig. 1e. The lattice spacing of 0.35 nm is attributed to the (101) crystal plane of TiO_2, and the lattice spacing of 0.19 nm corresponds to the (200) crystal plane [28]. It is important to see that TiO_2 is in good contact with the carbonized resin, forming a good interface. In Fig. 1f, the mapping spectrum of TCC also shows that the framework of CNTF contains three elements: C, O, and Ti, which proves that TiO_2 is successfully loaded on CNTF.

The photocatalytic activity was evaluated by the degradation of RhB under ultraviolet light irradiation. In Fig. 2a, the degradation efficiency of RhB by spraying CNTF with different layers of TiO_2 in 120 min was detected. Among them, 9TCC displayed remarkable photocatalytic activity, with a degradation rate of 91.29% in 120 min. We can see from Fig. 2b that the Rh B degradation effciencies over the pure TiO_2 was 63%. The degradation rate of 9TCC is 1.45 times that of pure TiO_2 powder. The phenomenon of CNTF has also been observed for comparison. Besides, the photocatalytic degradation reactions follow the first-order model (Langmuir–Hinshelwood kinetic) [29]: $-\ln(C_0/C) = kt$, where C_0 is the initial concentration, C is the concentration of RhB at the time t and k is the apparent rate constant. In Fig. 2c, the apparent reaction rates of 9TCC (0.0233 min^{-1}) was 2.7 times as high as that of pure TiO_2 (0.00859 min^{-1}). The UV absorption spectrum of RhB in Fig. 2d is consistent with the degradation curve of RhB by 9TCC. What is more, we conducted recycle experiments to evaluate the stability of the 9TCC. In Fig. 2e, the RhB could still reach 88% within 120 min after three cycles, indicating that it had good cycle stability. Organic carbon degradation efficiency is an important factor in the practical application of photocatalysts. In Fig. 2f, the TOC before and after 9TCC degradation of RhB are 8.07 mg/L and 3.09 mg/L, respectively, and the mineralization rate is 61.71%,

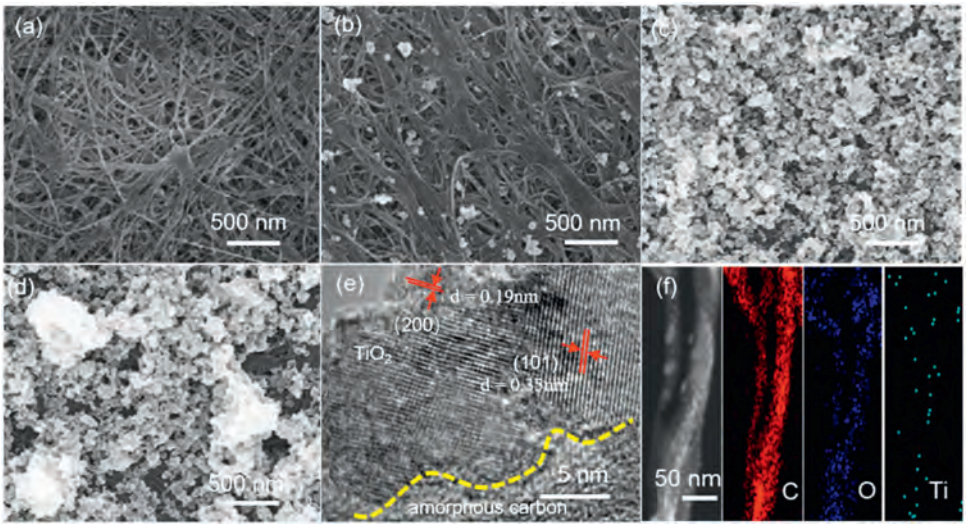

Fig. 1. SEM images of pure CNTF (a), 3TCC (b), 9TCC (c) and 11TCC (d). (e) HRTEM images of 9TCC. (f) Elemental mapping images of 9TCC.

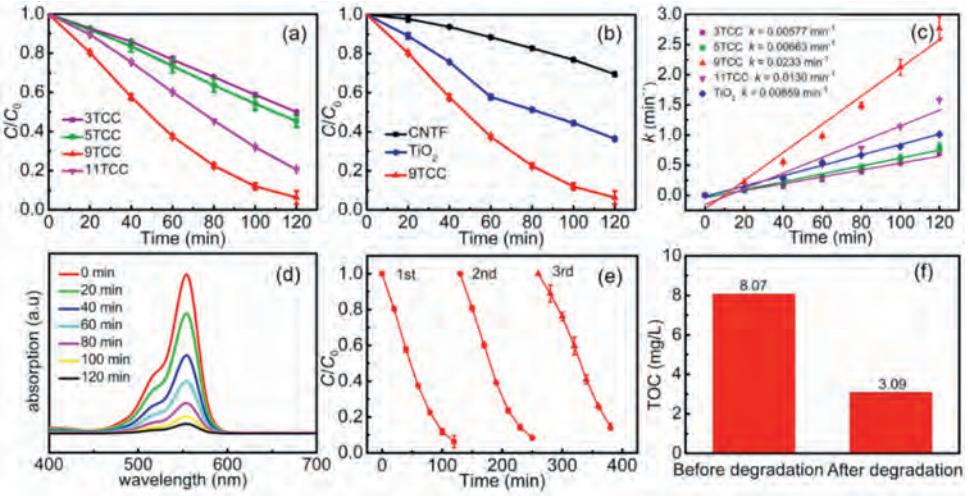

Fig. 2. Degradation of RhB by (a) TCC with different layers of TiO_2 and (b) CNTF, TiO_2, 9TCC. (c) First-order plots for the photo-degradation of RhB and (d) liquid phase UV spectrum of 9TCC. (e) Cycling test of 9TCC; (f) TOC of 9TCC before and after the photo-degradation test.

which proves that the composite membrane can completely mineralize most of RhB into H_2O and CO_2.

In general, the photocatalytic process mainly includes: (i) Light absorption, (ii) the generation and migration of electron-hole pairs and (iii) the redox reaction of active sites on the surface [30]. We will explore the reasons for the improvement of photocatalytic activity from these aspects. First, the light absorption properties of TiO_2 and 9TCC were researched by UV–vis diffuse reflectance spectroscopy. In Fig. 3a, it can be seen that the characteristic absorption edge of TiO_2 is about 400 nm, while 9TCC has a strong absorption of light and responds to light in the entire ultraviolet-visible region. The band gap can be calculated by the following formula [31]: $\alpha h\nu = A(h\nu - E_g)^{m/4}$, where α is the absorption coefficient, h is Planck's constant, A is constant, m depends on the semiconductor type. As shown in Fig. 3b, the calculated band gap width (E_g) of TiO_2 and 9TCC are 3.28 eV and 3.03 eV. The smaller band gap of 9TCC is beneficial to better utilization of light, in favor of improving the photocatalytic activity. In addition, the electrochemical impedance spectroscopy (EIS) and transient photocurrent response were also evaluated. Photocurrent refers to the situation in which electrons respond when the material is irradiated with light, and the electrons and holes are separated, migrate and form a current. Fig. 3c illustrates that TiO_2 and 9TCC can form a stable current under the irradiation of a 300 W xenon lamp. A higher current density of 9TCC was observed, indicating that it has better separation of electron-hole pairs, which is consistent with the photocatalytic degradation efficiency of RhB. In Fig. 3d, the Nyquist plots of 9TCC and TiO_2 are displayed. The equivalent circuit is shown in Fig. 3d in the upper left corner. R_s is the interface resistance between the photocatalyst and the carrier, R_e is the carrier migration resistance at the interface between the electrolyte and the counter electrode, and R_{ct} is the carrier migration resistance between the electrolyte and the photocatalyst. R_{ct} is an important parameter to characterize the photocatalytic activity [32,33]. From the relevant parameters of the equivalent circuit diagram (Table S1 in Supporting information), it can be observed that the R_{ct} of 9TCC is the smallest, indicating the lowest charge transfer resistance and the best separation of electron-hole pairs.

Finally, we conducted a photoluminescence (PL) spectrum and hydrophilicity test. The recombination of electrons and holes can be detected by PL spectrum after the electron transition from valence band to conduction band. In Fig. 3e, the PL spectrum shows that all materials have an emission peak at 370 nm. The stronger

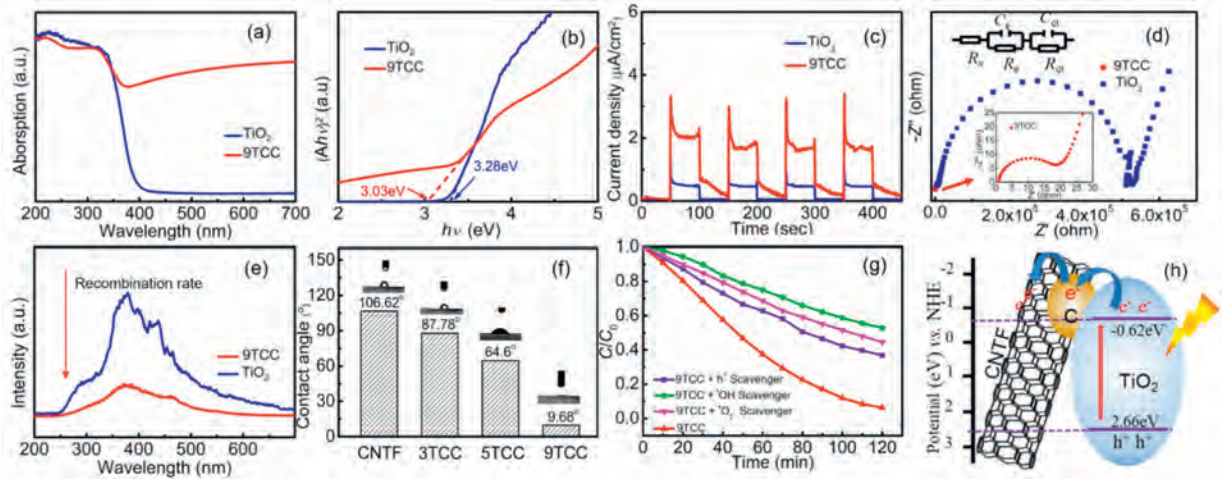

Fig. 3. (a) UV–vis-NIR diffuse-reflectance spectra and (b) converted Kubelka-Munk plot of TiO_2 and 9TCC. (c) Transient photocurrent response diagram and (d) Nyquist plots of TiO_2 and 9TCC. (e) PL emission spectra of TiO_2 and 9TCC. (f) Contact angle of 9TCC. (g) Photodegradable RhB with scavenger agent. (h) Schematic diagram of photocatalytic process of 9TCC.

emission peaks of TiO_2 at 370 nm. Compared with TiO_2, the peak of 9TCC is lower, which proves that it has a lower electron-hole recombination rate. According to reports, the hydrophilicity of the photocatalyst has a synergistic effect with the photocatalytic activity [34], so we measured the contact angle of TCC. In Fig. 3f, the contact angle of CNTF is 106.62°, and the contact angles of 3TCC, 5TCC and 9TCC are 87.78°, 64.6° and 9.68°, respectively. The improved wettability of the TCC composite is attributed to the hydroxyl group on the surface of TiO_2 [35]. The hydroxyl group can improve the wettability of the composite in aqueous solution, enhance the contact between the catalyst and the dye, and potentially increase the catalytic ability of the composite [36].

In order to verify the band gap positions of semiconductor, Mott-Schottky tests for TiO_2 and 9TCC were performed. Fig. S6a and b (Supporting information) presents that the slope of TiO_2 and 9TCC are positive, which are typical n-type semiconductor. The intercept between the Mott-schottky curve and the X-axis is the flat band potential (V_{FB}) of the semiconductor. The minimum value of the conduction band (CB) of the n-type semiconductor differs by 0.2 V from the respective V_{FB} [37]. Therefore, the CB of TiO_2 is −0.62 eV, and the VB is 2.66 eV calculated by $E_{CB} = E_{VB} - E_g$ [38]. The CB and VB of the 9TCC are −0.48 eV and 2.55 eV, respectively. In order to explore the main oxygen active substances in photocatalytic degradation, capture experiments were carried out with ammonium oxalate, *p*-benzoquinone and *tert*-butanol as scavengers for h^+, $^{\bullet}O_2^-$ and $^{\bullet}OH$. In Fig. 3g, the degradation rate of RhB with scavenger added is exhibited. The inhibitory effect of adding hydroxyl radical traps is the most obvious, which proves that $^{\bullet}OH$ is the main oxidizing species in the photodegradation process. Based on the above results, the photocatalytic mechanism of TCC is shown in Fig. 3h. The electrons of TiO_2 in VB can be excited to CB to form photo-excited electrons, producing photo-excited holes in VB. Amorphous carbon is used as an electron transport channel to migrate the photo-excited electrons of TiO_2 to the CNTF, which accelerating the separation efficiency of the photogenerated carries and enhancing the photocatalytic reaction. For RhB degradation, the VB potential of n-TiO_2 (E_{VB} =2.66 eV *vs.* NHE) can oxidize H_2O into $^{\bullet}OH$ ($E(^{\bullet}OH/H_2O)$ = 2.38 eV *vs.* NHE) [39]. Finally, RhB can be mineralized to CO_2 and H_2O by $^{\bullet}OH$.

RhB intermediates in photodegradation were analyzed by HPLC-MS (Table S2 in Supporting information). The degradation of RhB is shown in Fig. S7 (Supporting information) and begins with *N*-de-ethylation reaction. The *N*,*N*-diethylrhodamine (DR) and *N*-ethylrhodamine (EER) with *m/z* peaks of 415 and 387, and rhodamine, a completely de-ethylated product are detected. The discoloration of the RhB solution may be caused by the de-ethylation process [40]. This experiment can also detect phthalic anhydride and benzoic acid at the *m/z* peaks of 148 and 122, which proves that the oxygen-active species can further attack the carbon chain and cause a ring-opening reaction. Chain organic, such as oxalic acid, maleic acid and *p*-hydroxybenzoic acid [41]. Finally, the photocatalyst completely mineralizes small molecular organics into H_2O and CO_2, which is consistent with the result of TOC.

In this work, we prepared a novel TCC composite film for the degradation of RhB dyes. Compared with TiO_2, TCC composite film exhibited much enhanced photocatalytic activity. The CNTF can enhance light absorption to improve the separation and mobility of electrons and holes. The existence of amorphous carbon will promote these advances. Besides, the better hydrophilic properties would enhance the catalytic performance happened on the solid-liquid interface. In addition, we analyzed the degradation pathway of RhB by TCC based on the experimental results of TOC and HPLC-MS. The TCC composite film can oxidize the carbon on the benzene ring of RhB to decompose it into small organic molecules, and finally mineralize into H_2O and CO_2.

Declaration of competing interest

The authors declare that they have no known competing financial interests or personal relationships that could have appeared to influence the work reported in this paper.

Acknowledgments

This work is supported by the National Natural Science Foundation of China (Nos. 21872102 and 21906001).

Appendix A. Supplementary data

Supplementary material related to this article can be found, in the online version, at doi:https://doi.org/10.1016/j.cclet.2020.11.054.

References

[1] Z. Bian, F. Cao, J. Zhu, H. Li, Environ. Sci. Technol. 49 (2015) 2418–2424.
[2] F. Mashkoor, A. Nasar, J. Magn. Magn. Mater. 500 (2020) 166408.
[3] M. Ji, Z. Zhang, J. Xia, et al., Chin. Chem. Lett. 29 (2018) 805–810.
[4] S. He, C. Yan, X.Z. Chen, et al., Appl. Catal. B 276 (2020)119138.
[5] S. Hu, Y. Yu, Y. Guan, et al., Chin. Chem. Lett. 31 (2020) 2839–2842.
[6] F.C. Ferreira, R.S. Babu, A.L.F. de Barros, et al., Spectroc. Acta Part A 233 (2020) 118198.
[7] K. Ilić, A. Selmani, M. Milić, et al., J. Nanopart. Res. 22 (2020) 71.
[8] J. Krýsa, G. Waldner, H. Měšťánková, J. Jirkovský, G. Grabner, Appl. Catal. B 64 (2006) 290–301.
[9] S. Fukugaichi, T. Henmi, N. Matsue, Catal. Lett. 143 (2013) 1255–1259.
[10] H. Yu, S.C. Lee, J. Yu, C.H. Ao, J. Mol, Catal. A Chem. 246 (2006) 206–211.
[11] P. Karami, B. Khorshidi, M. McGregor, et al., J. Clean. Prod. 250 (2020) 119447.
[12] Y. Liu, J. Yin, P. Wang, et al., ACS Appl. Mater. Interfaces 10 (2018) 36304–36311.
[13] M. Zhu, M. Fujitsuka, L. Zeng, M. Liu, T. Majima, Appl. Catal. B 256 (2019) 117864.
[14] M. Wongaree, S. Chiarakorn, S. Chuangchote, T. Sagawa, Environ. Sci. Pollut. Res. 23 (2016) 21395–21406.
[15] T.V. Cuong, H.N. Tien, V.H. Luan, et al., Phys. Status Solidi A: Appl. Mat. 208 (2011) 943–946.
[16] M.S. Balogun, H. Yang, Y. Luo, et al., Energy Environ. Sci. 11 (2018) 1859–1869.
[17] Q. Liu, L. Ai, J. Jiang, J. Mater. Chem. A 6 (2018) 4102–4110.
[18] A. Jian, M. Wang, L. Wang, et al., RSC Adv. 9 (2019) 41540–41548.
[19] H. Liu, W. Li, D. Shen, D. Zhao, G. Wang, J. Am. Chem. Soc. 137 (2015) 13161–13166.
[20] H. Yin, X. Wang, L. Wang, et al., Mater. Res. Bull. 72 (2015) 176–183.
[21] T. Onoe, S. Iwamoto, M. Inoue, Catal. Commun. 8 (2007) 701–706.
[22] H.U. Farouk, A.A.A. Raman, W.M.A.W. Daud, J. Ind. Eng. Chem. 33 (2016) 11–21.
[23] M.M. Hossain, H. Shima, M.A. Islam, M. Hasan, M. Lee, J. Phys. Chem. C 120 (2016) 17670–17682.
[24] J.Y. Kim, Materials 2 (2009) 1955–1974.
[25] N. Ohtsu, N. Masahashi, Y. Mizukoshi, K. Wagatsuma, Langmuir 25 (2009) 11586–11591.
[26] M.E. Simonsen, Z. Li, E.G. Søgaard, Appl. Surf. Sci. 255 (2009) 8054–8062.
[27] B. Gong, X. Luo, N. Bao, et al., Surf. Interface Anal. 46 (2014) 1043–1046.
[28] F. Boccuzzi, A. Chiorino, M. Manzoli, et al., J. Catal. 202 (2001) 256–267.
[29] Z. Wei, Y. Liu, J. Wang, et al., Nanoscale 7 (2015) 13943–13950.
[30] B. Li, Z. Cao, S. Wang, Q. Wei, Z. Shen, Dalton Trans. 47 (2018) 10288–10298.
[31] H. Wang, X. Yuan, Y. Wu, et al., Appl. Catal. B 186 (2016) 19–29.
[32] Y. Zhang, Z. Shen, Z. Xin, Z. Hu, H. Ji, J. Colloid Interface Sci. 554 (2019) 743–751.
[33] J. Duan, Q. Tang, B. He, L. Yu, Electrochim. Acta 139 (2014) 381–385.
[34] Y.S. Li, T.T. Li, X.F. Song, et al., Appl. Surf. Sci. 514 (2020) 145789.
[35] R. Mimouni, B. Askri, T. Larbi, M. Amlouk, A. Meftah, Inorg. Chem. Commun. 115 (2020)107889.
[36] Z. Li, H. Dong, Z. Wu, et al., Appl. Surf. Sci. 529 (2020) 147162.
[37] D. Jiang, L. Chen, J. Zhu, et al., Dalton Trans. 42 (2013) 15726–15734.
[38] X. Wu, M. Li, J. Li, G. Zhang, S. Yin, Appl. Catal. B 219 (2017) 132–141.
[39] Y. Chen, J.F. Li, P.Y. Liao, et al., Chin. Chem. Lett. 31 (2020) 1516–1519.
[40] N. Guo, H. Liu, Y. Fu, J. Hu, Optik 201 (2020) 163537.
[41] G. Sharma, D.D. Dionysiou, S. Sharma, et al., Catal. Today 335 (2019) 437–451.